OPEN ACCESS

Environment & Ecology ARTICLE

Temperature shapes spatial-temporal patterns of global soil carbon accumulation

Shanshan Yang,[1,7] Juan Li,[1,7] Yakov Kuzyakov,[2,3] Pete Smith,[4] Lixin Wang,[5] Yafeng Wang,[1] Shuai Ren,[6] Huangyu Huo,[1] Xiling Gu,[1] Miaoyue Wang,[1,5] Jiayi Li,[1] Hao Cheng,[1,5] and Jinzhi Ding[1,*]

*Correspondence: jzding@itpcas.ac.cn

Received: June 16, 2025; Accepted: March 11, 2026; Published Online: March 16, 2026; https://doi.org/10.59717/j.xinn-geo.2026.100214

GRAPHICAL ABSTRACT

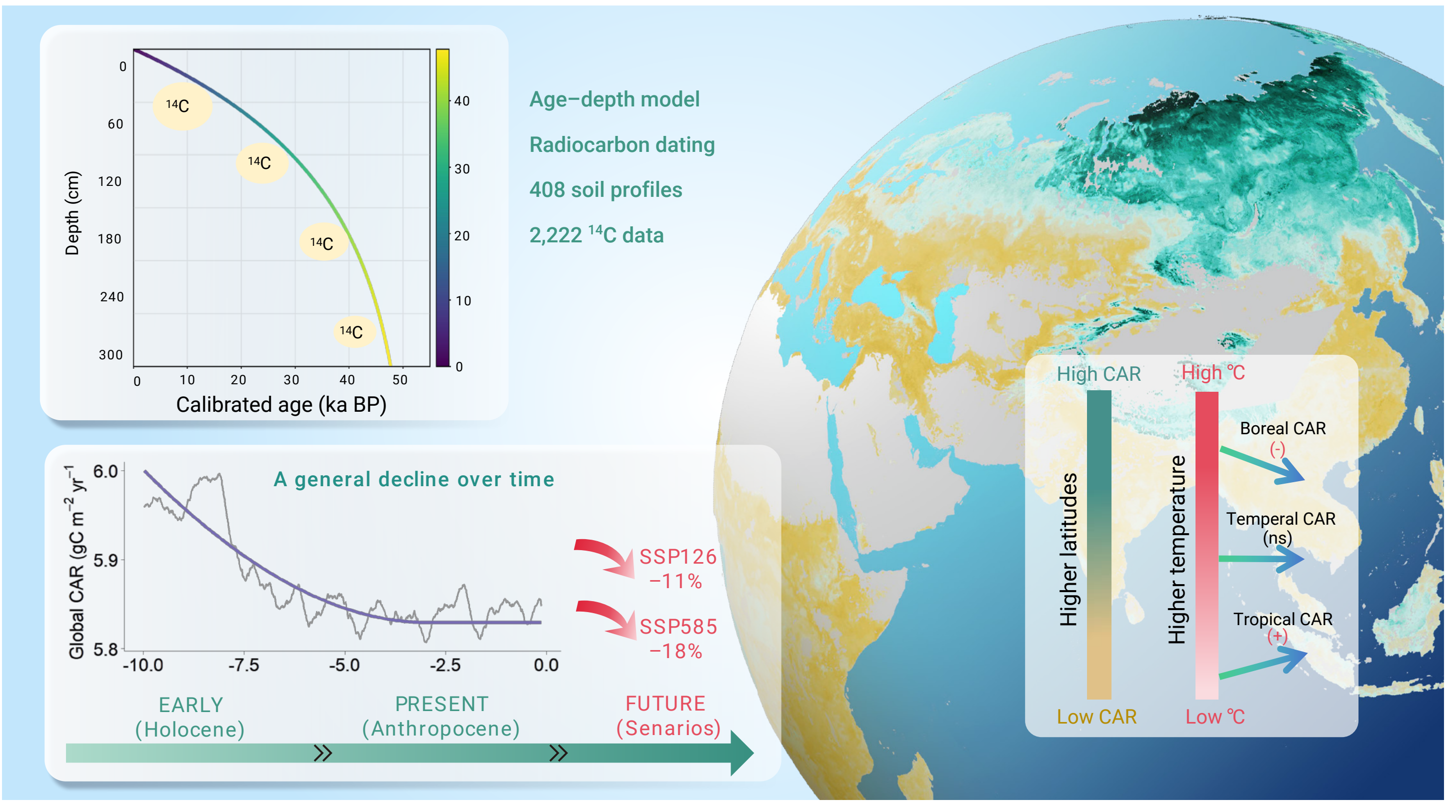

PUBLIC SUMMARY

- Global carbon accumulation rate (CAR) is reconstructed from 2,222 radiocarbon dates across 408 soil profiles.
- CAR trajectory is non-linear and biome-specific over millennia.
- Temperature dominates global CAR patterns, with higher spatial than temporal temperature sensitivity.
- High-latitude regions show the highest historical CAR but are most vulnerable to climate change.
- CAR has declined since the early Holocene and is projected to decline further (−11% SSP126; −18% SSP585).

Temperature shapes spatial-temporal patterns of global soil carbon accumulation

Shanshan Yang,[1,7] Juan Li,[1,7] Yakov Kuzyakov,[2,3] Pete Smith,[4] Lixin Wang,[5] Yafeng Wang,[1] Shuai Ren,[6] Huangyu Huo,[1] Xiling Gu,[1] Miaoyue Wang,[1,5] Jiayi Li,[1] Hao Cheng,[1,5] and Jinzhi Ding[1,*]

[1]State Key Laboratory of Tibetan Plateau Earth System, Environment and Resources (TPESER), Institute of Tibetan Plateau Research, CAS, Beijing 100101, China

[2]Department of Soil Science of Temperate Ecosystems, Department of Agricultural Soil Science, University of Göttingen, Göttingen 37077, Germany

[3]Peoples Friendship University of Russia (RUDN University), Moscow 117198, Russia

[4]Institute of Biological and Environmental Sciences, School of Biological Sciences, University of Aberdeen, Scotland, Aberdeen AB24 3UU, UK

[5]College of Ecology and Environment, Inner Mongolia University, Hohhot 010021, China

[6]Department of Civil and Environmental Engineering, Massachusetts Institute of Technology, Cambridge, MA 02139, USA

[7]These authors contributed equally

*Correspondence: jzding@itpcas.ac.cn

Received: June 16, 2025; Accepted: March 11, 2026; Published Online: March 16, 2026; https://doi.org/10.59717/j.xinn-geo.2026.100214

Citation: Yang S., Li J., Kuzyakov Y., et al. (2026). Temperature shapes spatial-temporal patterns of global soil carbon accumulation. *The Innovation Geoscience* **4**:100214.

Mitigation of climate change and maintenance of ecosystem functions highlight the great importance of carbon sequestration in soil, which is a long-term process ongoing over decades, centuries, and even millennia. Here we compiled 2,222 radiocarbon (^{14}C) measurements of soil organic matter from 408 soil profiles spanning all major biomes and coupled radiocarbon-based chronology with a chronosequence framework to reconstruct soil carbon accumulation since the early Holocene. This millennial-scale reconstruction captures long-term, non-linear trajectories and biome-dependent patterns over the Holocene. Our findings indicate that temperature was the dominant factor shaping the global spatial and temporal patterns of the carbon accumulation rate (CAR). Notably, the spatial sensitivity of CAR to temperature was nearly twofold greater than the within-profile temporal sensitivity, indicating that spatial gradients alone do not fully represent the magnitude of long-term temperature responses. Globally, CAR declines from the early Holocene to the present (Anthropocene) and is projected to decrease further by 11% under the SSP126 scenario and by 18% under the SSP585 scenario. High-latitude permafrost and wetland soils show the highest historical CAR but also the largest projected declines, whereas tropical soils exhibit a positive CAR–temperature relationship, which may reflect warming-associated increases in plant and root carbon inputs over long timescales. This radiocarbon-constrained CAR reconstruction provides an observation-based benchmark for evaluating Earth system models and highlights the increasing vulnerability of high-latitude soil carbon reservoirs under ongoing warming.

INTRODUCTION

The current global emphasis on climate change adaptation and mitigation has resulted in an unprecedented focus on soil carbon dynamics.[1] Soils constitute Earth's largest biologically active carbon reservoir, serving as the primary interface for terrestrial-atmospheric carbon exchange.[2] Their sensitivity to environmental changes renders even subtle carbon pool fluctuations potentially consequential, capable of raising atmospheric CO_2 concentrations and accelerating climate warming.[3–6] Currently, researchers have raised concerns regarding the vulnerability of soil carbon reservoirs under climate changes. This concern arises from the anticipated acceleration of microbial respiration rate under warming, leading to the depletion of soil carbon and positive carbon-climate feedback loops.[5,7] Simultaneously, higher temperatures may extend the growing season and facilitate plant photosynthesis, thereby increasing vegetation productivity and the influx of plant-derived carbon into soils.[6,8] The overall impact of these combined effects on soil carbon sequestration rate remains largely uncertain, with a lack of consensus among studies.

The scientific community has employed diverse methodologies to unravel these complex interactions, including field-warming experiments,[9] direct measurements of soil carbon stocks,[10] model simulations,[11] and other methodologies,[12] summarized in Soldatova et al.[13] However, significant limitations persist in current approaches. Most field studies, typically spanning one to several decades, predominantly extrapolate warming effects through organic matter decomposition rates, a methodology that introduces many inaccuracies in predictions as decomposition responses do not necessarily align with changes in soil carbon stocks.[14] These constraints are particularly incongruous with soil carbon's millennial-scale accumulation history and its inherent lagged response to climatic variations. Pedological evidence and radiocarbon dating reveal that surface soil carbon averages 5,000 years in age, with permafrost regions preserving carbon reservoirs dating beyond ten millennia.[15,16] This temporal discordance between observational scales and soil carbon's inherent timescales presents a fundamental scientific challenge. Most short-term studies constrain rapid flux responses to climate change, whereas soil carbon sequestration reflects the long-term imbalance between carbon inputs and losses. Over longer timescales, warming may enhance vegetation productivity and thus increase carbon inputs, potentially offsetting part of the warming-related carbon losses. Therefore, conventional short-term observations provide only a partial view of the processes that shape carbon sequestration on multi-millennial timescales.

Recognizing this scale mismatch, long-term experimental platforms and modelling frameworks have been developed to extend beyond short-term observations.[17,18] Long-term perspectives on soil carbon dynamics have been mainly derived from peat and lake-sediment records, site-level chronosequences, regional to global stock reconstructions, and process-based Earth system models (ESMs).[19,20] Paleoecological archives such as peat and lake sediments provide valuable long-term information, but they are restricted to specific depositional environments and rarely yield continuous, depth-resolved and globally comparable reconstructions of soil C accumulation rates across diverse biomes.[21–23] Likewise, although ESMs can simulate soil C dynamics over millennial timescales, their parameterization and evaluation still rely heavily on short-term observations, which may introduce substantial uncertainty into long-term projections of global soil carbon dynamics.[24,25] Recent global syntheses of soil radiocarbon have greatly improved constraints on the age distribution and persistence of soil organic carbon.[16,26,27] However, these syntheses have not been used to estimate soil CAR or to quantify its climate sensitivity across biomes. Moreover, they provide limited insight into whether the sensitivity inferred from spatial patterns aligns with that expressed through time in millennial-scale CAR. Therefore, we still lack a global, radiocarbon-constrained reconstruction of millennial-scale soil carbon accumulation, limiting our ability to characterize long-term, non-linear trajectories and biome-dependent patterns that are critical for understanding carbon–climate feedbacks.

To bridge this gap, we compiled a global dataset of 2,222 ^{14}C measurements from 408 soil profiles spanning all major biomes (Figure S1) and coupled radiocarbon-based chronology with a chronosequence framework to reconstruct Holocene CAR. This framework allows us to (1) evaluate spatiotemporal patterns in soil carbon accumulation rates since the early Holocene, (2) identify key determinants of these accumulation processes, and (3) develop predictive insights about soil carbon responses to future climate scenarios. Accordingly, we hypothesized that soil carbon accumulation rates (CAR) would exhibit distinct spatial and temporal patterns along major climatic and biogeographic gradients, and that climate acts as the primary

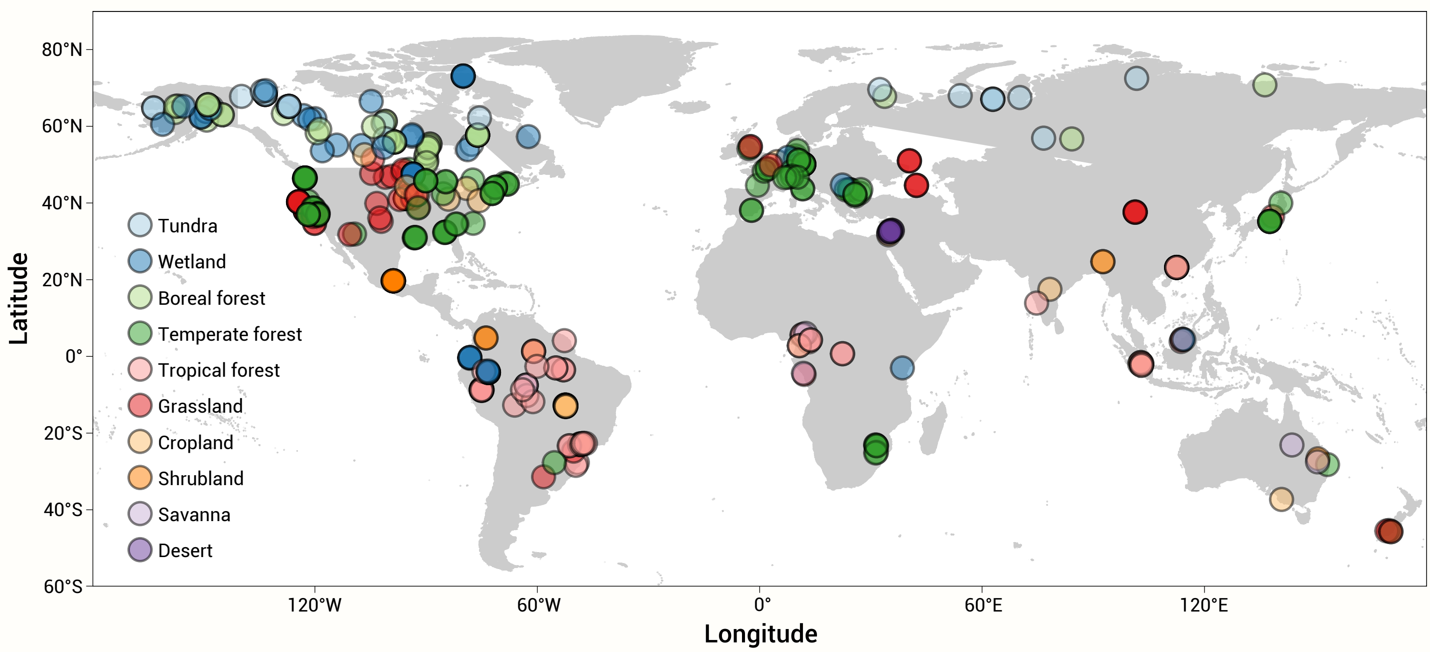

Figure 1. Global distribution of the 408 sampling sites Circle colors indicate biomes.

control on this global variation in CAR, because of its fundamental constraints on both plant productivity (carbon input) and microbial decomposition (carbon output). Based on these considerations, we further expect that ongoing anthropogenic warming will tend to reduce global CAR, with the most pronounced decreases in high-latitude regions where large, temperature-sensitive C stocks are currently sequestered. By establishing this millennial-scale perspective, we aim to advance understanding of carbon-climate feedback mechanisms and inform adaptive strategies for soil carbon management in the context of global climate change.

MATERIALS AND METHODS

Data compilation

Soil $\Delta^{14}C$ dataset was obtained from ISRaD, an open community repository for soil radiocarbon data[28] supplemented by searching key words "radiocarbon" and "$\Delta^{14}C$" on "Web of Science", we compiled a global $\Delta^{14}C$ dataset. Soil profiles with unreasonable data were eliminated, such as negative depth values, extreme $\Delta^{14}C$ values (i.e., calibrated calendar years later than the sample's collection year), and soil profiles with less than three sampling depths.[29,30] Finally, there was a total of 2,222 unique $\Delta^{14}C$ values measured at different depths of 408 soil profiles. Each soil profile had at least three individual samples at different depths and all soil profiles were distributed globally, covering various vegetation types and biomes (Figures 1–2 & S1). Other corresponding information was also collected, such as sampling/publication year, site location (i.e., longitude and latitude), soil depths, and land cover types (i.e., tundra, wetland, boreal forest, temperate forest, tropical forest, grassland, cropland, shrubland, savanna and desert).

For the global extrapolation, 18 auxiliary variables were obtained from multiple sources based on the geographical coordinates of each profile location. Climatic variables, i.e., mean annual temperature (Mean_T, °C), minimum temperature (Min_T, °C), maximum temperature (Max_T, °C) and mean annual precipitation (Precip., mm) were obtained from the global climate database—WorldClim at ~1 km resolution for contemporary climate (1970–2000)[31] and based on PaleoView v1.0 tool for decadal paleoclimate at ~55 km resolution.[32] Global gridded photosynthetically active radiation (PAR, $W \cdot m^{-2}$) at ~10 km and 3-hourly resolution were obtained from the National Tibetan Plateau Data Center (TPDC),[33] annual growing season length (GSL, days) at 500 m resolution was obtained from MODIS phenology product (MCD12Q2-EV12),[34] then the mean photosynthetically active radiation over the growing season was determined accordingly. Aridity index (AI), defined as the ratio of annual precipitation to annual potential evapotranspiration, was provided by Global Aridity Index and Potential Evapotranspiration Climate Database v3 at ~1 km resolution.[35] Net primary productivity (NPP, $g \cdot C \cdot m^{-2} \cdot yr^{-1}$) was extracted from MODIS annual NPP product (MOD17A3) at ~1 km resolution.[36] Belowground biomass carbon (BGB, Mg C ha^{-1}) was extracted from the harmonized global maps of belowground biomass carbon density for the year 2010 at ~300 m resolution.[37] Topographic variables, i.e., slope and elevation, were derived from Digital Elevation Models (DEMs) at 30 m resolution.[38] Variables associated with soil properties, i.e., pH, clay content (%), cation exchange capacity (CEC, $cmol \cdot kg^{-1}$), were obtained from the SoilGrids250m v.2.0 database at 250 m resolution.[39,40] For each site, values of soil properties were aggregated to 0–200 cm by taking the mean of different soil layers (0–5, 5–15, 15–30, 30–60, 60–100, 100–200 cm). Microbial variables, i.e., fungal biomass carbon (FBC, $g \cdot C \cdot m^{-2}$), bacterial biomass carbon (BBC, $g \cdot C \cdot m^{-2}$), ratio of fungal to bacterial biomass carbon (F:Bratio), and microbial residence time (MRT) at ~55 km resolution were extracted from published literature.[41,42] The gridded variables used for the global extrapolation were resampled to a 500 m grid using bilinear interpolation.

Chronology and soil age–depth modelling

Based on the global $\Delta^{14}C$ dataset, we converted $F^{14}C$ into $\Delta^{14}C$ to standardize the radiocarbon reporting nomenclature according to the following equations:[43]

$$\Delta^{14}C = \left[F^{14}C \times \exp\left(\frac{-(y-1950)}{8267} \right) - 1 \right] \times 1000 \qquad (1)$$

Where "$F^{14}C$" is a common term used for reporting ^{14}C activity,[44] and "y" refers to sampling year. The constant 8267 is the true mean life of radiocarbon. Notably, when sampling year is not available, "y" is assumed to be the publication year minus three considering the mean-time interval between sampling and publication reported in literature.[16] Most of the studied sampling sites are open systems, plants may contribute to new organic carbon supply across different soil depths during the development of most soils, especially for the top one meter.[45,46] Therefore, to convert $\Delta^{14}C$ into soil carbon age with the consideration of the vertical C transport along the soil profile, we applied a one-pool radiocarbon model using the time series of atmospheric $\Delta^{14}C$ over the past 50 kyr.[47–49]

We performed age–depth models for each profile using BACON v2.3.9.1 package in R version 3.4.3[50] to provide timescales over which the carbon measured down-core had accumulated.[51] Specifically, Bacon utilizes Bayesian statistics to reconstruct the soil accumulation histories by dividing each profile into equally-sized sections and estimating accumulation rates for each section. Prior information on sedimentation rates and their variability

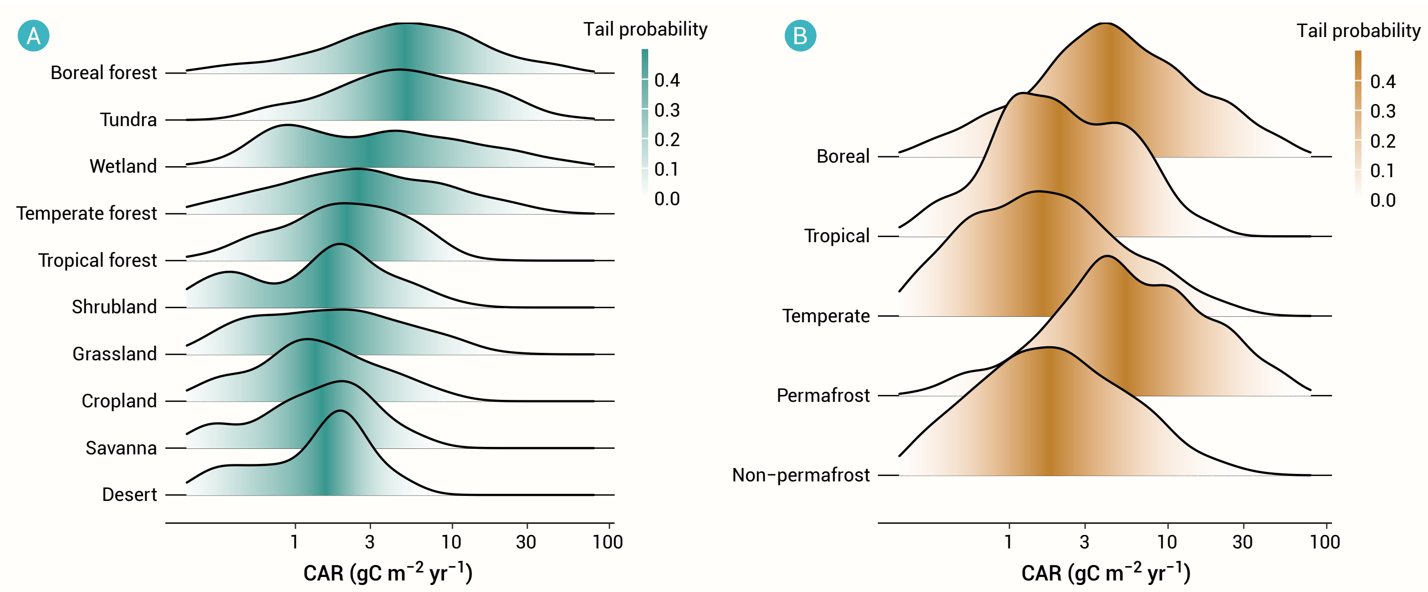

Figure 2. Density distributions of soil carbon accumulation rate (CAR) across ecosystems (A) and across climate zones and permafrost regions (B) Color intensity indicates the probability density of CAR values on a logarithmic scale, with darker colors representing higher densities.

was incorporated into the model using a gamma distribution, parameterized by a mean accumulation rate and its variability. The priors were set based on initial stratigraphic assessments and adjusted to achieve model convergence. Millions of Markov Chain Monte Carlo (MCMC) iterations were run to generate posterior distributions of both age and accumulation rates. The soil accumulation rates (SAR, $yr \cdot cm^{-1}$) were estimated through millions of Markov Chain Monte Carlo (MCMC) iterations. After each Bacon model run, three datasets were generated, i.e., ^{14}C ages along with their error distribution, the data forming the age–depth model, and the accumulation rate (Figure S2). Bayesian framework allows extrapolation of accumulation rates to depths beyond the range of dated points, with associated uncertainty estimates. In this study, soil profiles varied in sampling depths, ranging from 0 to 300 cm, although most profiles were less than 100 cm deep (Figure S1). To facilitate comparison across profiles, we standardized all age–depth models by extrapolating them to a depth of 100 cm, ensuring consistency in data integration and interpretation.

Carbon accumulation rate determination

The BACON–estimated soil accumulation rates (SARs) were used to calculate the carbon accumulation rates (CARs) for each profile. CAR was calculated according to the following equation:[22,52-53]

$$\text{CAR}\ (\text{gC m}^{-2}\text{yr}^{-1}) = \frac{\sum_{i=1}^{100} \text{SOCD}_i\ (\text{gC m}^{-2})}{1\ \text{m}} \times \text{SAR}\ (\text{m yr}^{-1}) \tag{2}$$

Where "i" refers to a specific soil layer (cm). "CAR" is the mean carbon accumulation rate of the top 1 m (0–100 cm) soil profile ($g \cdot C \cdot m^{-2} \cdot yr^{-1}$). "SOCD" is the soil organic carbon density calculated by multiplying bulk density (BD, $g\ cm^{-3}$), soil organic carbon content (SOCC, $g\ kg^{-1}$), soil horizon thickness (T, cm), and the volume percentage of gravel (> 2 mm, C, %), which are sourced from the World Soil Information Service (WoSIS)[54] and published literature.[55,56] We then mapped SOCD at 1-cm vertical resolution (0–100 cm) using the predictive framework of Li et al.[27] "SAR" is vertical soil accumulation rate ($m \cdot yr^{-1}$) generated from above Bayesian age–depth models.

We also used three other auxiliary calculation methods to explore global soil carbon accumulation rates (Figure S3). These three methods were: (a) linear regression model;[29,57,58] (b) non-linear regression model with information of annual carbon input and organic carbon decomposition rate;[59,60] (c) CLAM age–depth model.[53,61] Specifically, for linear regression model, the mean carbon accumulation rate was the total carbon storage of the soil profile divided by the corresponding accumulation time, i.e. the median age difference between the top and bottom layers derived from age–depth models. To provide additional insight into the mechanisms behind CAR changes over time, a non-linear regression model was built. This model assumed that the net change in carbon storage was determined by the balance between carbon inputs and decomposition, and could only obtain the mean carbon accumulation rate of the whole soil profile according to the following equations:

$$\text{CAR} = \text{I} - \text{kC}_{\Delta t} \tag{3}$$

$$C_{\Delta t} = (I/k) \times (1 - e^{-k \cdot \Delta t}) \tag{4}$$

Where "$C_{\Delta t}$" is the variation in organic soil carbon inventory during year Δt. "*I*" is the annual carbon inputs ($g \cdot C \cdot m^{-2} \cdot yr^{-1}$). "*k*" is the first-order decomposition constant in yr^{-1}. We can also obtain the values of annual carbon input and output (i.e., organic carbon mineralization) of corresponding soil profile. The CLAM classical age–depth model was one of the widely used age–depth models and most cited before 2016.[30] This age–depth model for each profile was conducted with the software CLAM v2.3.5 in the programming language R.[61] Notably, extrapolation beyond the ^{14}C dated levels is inadvisable but can be done if required, here linear interpolation between neighboring levels was chosen to estimate the ages of the non-dated levels, and we extrapolated beyond the dated levels to a soil depth of 100 cm. Among the four described approaches (Figure S3), BACON was chosen and its outputs were presented and discussed in the main text, while other three approaches were only shown in Supplementary Materials as auxiliary approaches. Here we chose BACON model because of its higher precision in age estimation throughout the profile,[30] and even at low dating densities, Bayesian models are preferable to classical models because their model assumptions produce more realistic reconstructions and confidence intervals.[62]

Statistical analyses

Global mapping of soil carbon accumulation rate. To assess the fundamental drivers of variation in soil CAR and predict the global patterns of CAR, we ran random forest (RF) models with the R package "*randomForest*"[63] in the R statistical language.[50] The random forest is an ensemble machine learning algorithm that consists of an ensemble of randomized classification and regression trees (CART).[64] Each decision tree is trained on a subset of the data, and the predictions of all the trees are averaged to produce the final prediction, which makes RF robust to overfitting and able to handle complex relationships between the explanatory variables and the response variable.[65] In total 18 variables associated with climate, vegetation, soil property, topography, and organisms were derived from the original studies or global map layers (details were described above) and treated as explanatory variables,

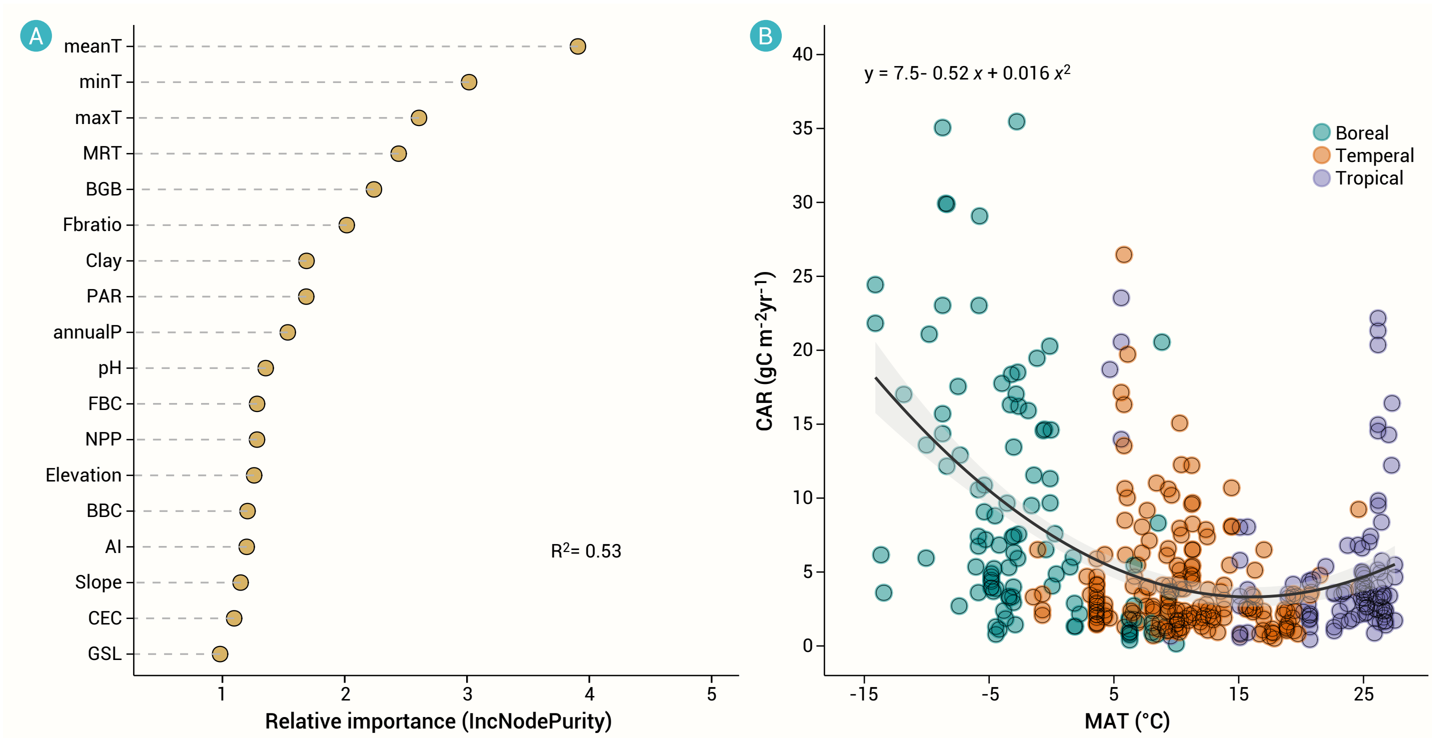

Figure 3. Drivers of temporal and spatial patterns of soil carbon accumulation rate (CAR) (A) Relative importance of factors predicting the spatial pattern of soil CAR using a random forest model. (B) Spatial relationship between mean annual temperature (MAT) and the one-meter-depth average soil CAR of the 408 sampling sites. The abbreviations in panel A indicate the predictor variables, that is, meanT, mean annual temperature (°C); minT, minimum annual temperature (°C); MRT, microbial residence time (days); maxT, maximum annual temperature (°C); annualP, mean annual precipitation (mm); Fbratio, fungal to bacterial ratio ($g{\cdot}C{\cdot}m^{-2}$); NPP, net primary productivity ($g{\cdot}C{\cdot}m^{-2}{\cdot}yr^{-1}$); BGB, below-ground biomass ($Mg{\cdot}C{\cdot}ha^{-1}$); PAR, photosynthetically active radiation over the growing season ($\mu mol{\cdot}m^{-2}{\cdot}s^{-1}$); Clay, clay soil content (%); BBC, bacterial biomass carbon ($g{\cdot}C{\cdot}m^{-2}$); AI, aridity index; CEC, cation exchange capacity ($cmol{\cdot}kg^{-1}$); FBC, fungal biomass carbon ($g{\cdot}C{\cdot}m^{-2}$); GSL, growing season length (days).

while CAR as response variable. Model performance was evaluated with leave-one-out cross-validation (LOOCV), in which each observation was held out once for testing, while the remaining *(n−1)* observations were used for training. LOOCV systematically enumerates all leave-one-out splits, thereby avoiding dependence on any single train–validation split. Performance metrics (R^2, RMSE) were averaged across all *n* folds. The final RF models were used to generate a spatially-explicit map at a global scale for the top 100 cm soil depth, and the standard deviation across all the RF models was then considered to be an indication of the prediction uncertainty. All variable layers were projected and resampled to the same resolution (0.05° spatial resolution) with the "*raster*" package before modelling.

RF allowed us to explore the effect of each individual variable on CAR, we therefore generated partial dependence plots (Figure S4) to visualize the effect of each explanatory variable on CAR, while accounting for the average effect of all other variables.[66] We further ranked the relative importance of all predictors based on the increased node purity, and found that climatic variables, especially temperature variables, outweighed other predictors and illustrated to be the most important explanatory variables in predicting soil carbon accumulation rate (Figure 3A).

Climate control on soil carbon accumulation rate. Random Forest analysis identified temperature as the dominant predictor of CAR (Figure 3A). To eliminate the bias caused by spatial variation of sampling sites, we fitted linear mixed-effects models (LMMs) to determine the effect of mean annual temperature (MAT) on soil carbon accumulation rate (CAR) for the global scale, temperature zones, and regions, with MAT fitted as a fixed-effects factor and sampling site as random effect. The effect of MAT was considered to be significant if $p < 0.05$. Mean change rate in log-transformed CAR in response to MAT with 95% confidence intervals (CI) was obtained from the LMM. This analysis was performed with the '*lme4*' package in the software R version 3.4.1.[67]

Temporal dynamics of soil organic carbon accumulation rate. Random forest (RF) models were also applied to predict the spatial-temporal patterns of CAR by substituting the determining and time-varying factors. In this study, we identified climate as the primary driver. Other variables such as inherent soil properties and topography remain relatively stable[68–70] and lack globally consistent time-series datasets.[71] Therefore, we used a climate-only perturbation framework with non-climatic variables held constant for projections. Specifically, we extracted past climatic factors (Min_T, Mean_T, Max_T, and Percip.) since the early Holocene for backward predictions,[32] and also extracted the corresponding future (i.e., 2100 AD) climatic factors at two climate scenarios (i.e., SSP126 and SSP585) from WorldClim v2.0 for forward predictions.[31] Therefore, we conducted RF models by replacing contemporary climate data with extracted time-varying ones, then global maps were generated to show the temporal dynamics of soil organic carbon accumulation rate. We further quantified the relative change in CAR over time by calculating the percentage difference (%) between predicted past/future CAR and present estimated CAR.

RESULTS

Faster historic carbon accumulation observed in high-latitude areas

Based on the compiled global measurements of soil ^{14}C and soil organic carbon density (SOCD) (Figure S1), we used age–depth models to determine soil accumulation rates and then calculated mean CAR for each profile. The mean CAR down to a depth of one meter varied from 0.94 to 30.0 $g{\cdot}C{\cdot}m^{-2}{\cdot}yr^{-1}$. Faster rates were observed in cold-anoxic regions, such as tundra, wetland, and boreal forest ecosystems, while slower rates were found in desert regions (Figure 2). Permafrost regions exhibited the highest soil CAR at 10.1 $g{\cdot}C{\cdot}m^{-2}{\cdot}yr^{-1}$, more than three times that of non-permafrost regions (3.2 $g{\cdot}C{\cdot}m^{-2}{\cdot}yr^{-1}$). The high-latitude cold zone demonstrated the highest soil CAR at 8.4 $g{\cdot}C{\cdot}m^{-2}{\cdot}yr^{-1}$, surpassing the tropical (3.3 $g{\cdot}C{\cdot}m^{-2}{\cdot}yr^{-1}$) and temperate zones (3.1 $g{\cdot}C{\cdot}m^{-2}{\cdot}yr^{-1}$) in mid-low latitudes. These latitudinal gradients of CARs were consistent with comparisons among ecosystems in terms of annual carbon inputs and outputs (Figures S5 & S6). Based on the estimated average carbon input and decomposition constant (represented by *I* and *k*), boreal forests, tundra, and wetlands in cold regions had decomposition constants (*k*) that were less than half of those in temperate or tropical areas for equivalent levels of carbon input (*I*) (Figures S5 & S6).

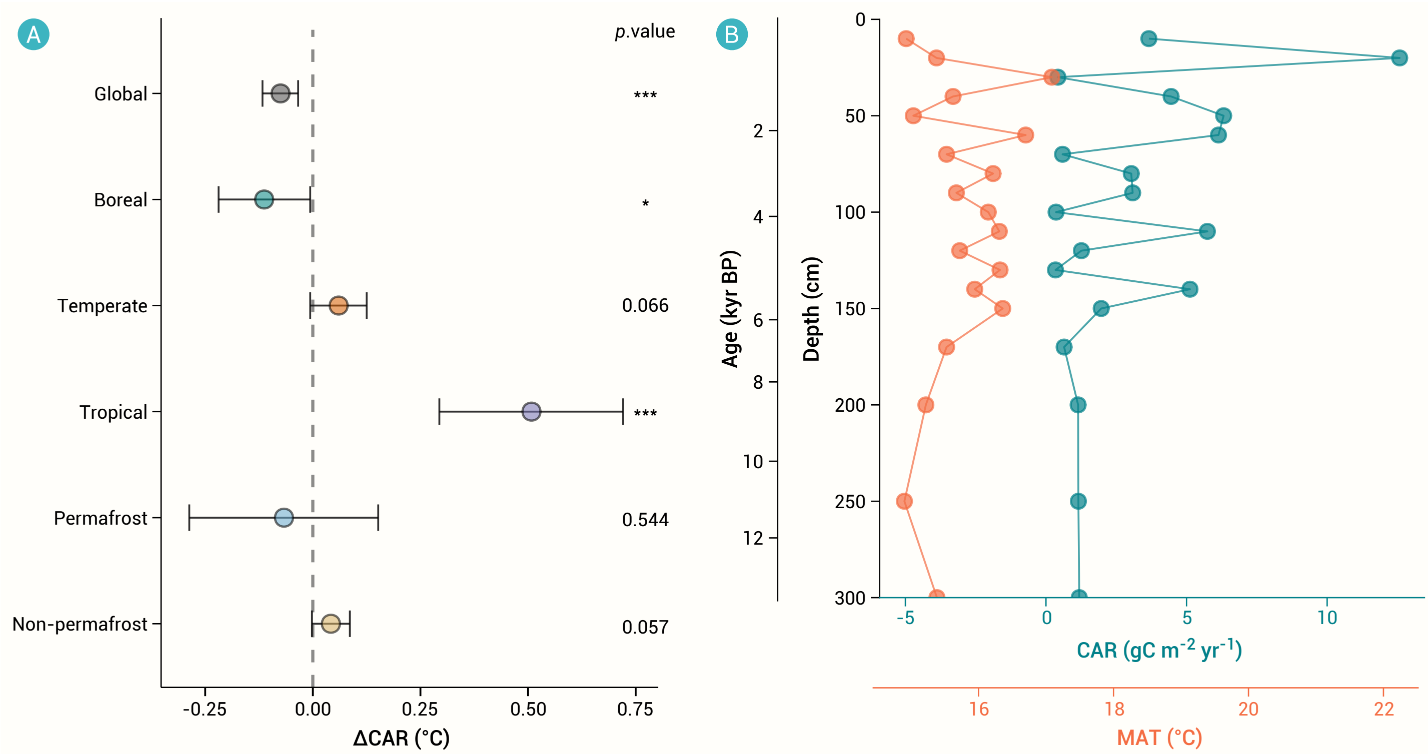

Figure 4. Temperature sensitivity of soil carbon accumulation rate (CAR) (A) Temporal response of CAR to changes in mean annual temperature estimated from 2,222 paired CAR–temperature observations derived from 408 soil profiles using linear mixed-effects models. The x-axis shows the mean temperature sensitivity of CAR (g C m^{-2} yr^{-1} °C^{-1}); error bars denote 95% confidence intervals (CI). Asterisks indicate statistical significance: * $p < 0.05$; ** $p < 0.01$; *** $p < 0.001$. (B) One typical soil profile illustrates the variation in paleo-temperature and CAR along soil depth, corresponding to different ages of soil organic carbon.

Temperature shapes spatio-temporal patterns of global CARs

The accumulation of carbon in the form of organic matter is involved in soil development over millennia,[21,72] and is controlled by biotic and abiotic factors.[73,74] To explore the importance of various variables on carbon accumulation, we conducted RF models incorporating 18 variables characterizing climate, vegetation, soil properties, microbial community and topography. Climatic variables, especially temperature, outweighed other predictors and illustrated the highest level of significance in explaining the global spatial distribution of soil CARs (Figure 3A). We further utilized correlation analysis and the outputs of partial dependence plots to visualize the independent contribution of each explanatory variable to CARs while controlling for the effects of other variables (Figure S4). Higher temperatures correlated with lower soil CARs on the global scale (Figures S4A–C). This adverse temperature effect on CARs was especially pronounced in a colder climate (where mean annual temperature, MAT was below 10°C), where CARs decreased more steeply with increasing temperatures. Conversely, in warmer regions, the inverse relationship between these two variables was less pronounced (Figure 3B). The spatial sensitivity of CAR to temperature, reflecting the variation in soil carbon accumulation rates across temperature gradients, was calculated to be −0.22 (95% confidence interval: −0.28, −0.17) g·C·m^{-2}·yr^{-1}·°C^{-1} (Table S1). These findings indicated that temperature played the main role in shaping the global spatial distribution of CARs.

The vertical profile of the soil carbon age provided an ideal alternative to examine the historical trajectory of carbon accumulation over time. Linear mixed models were conducted to investigate the relationship between the carbon accumulation dynamics and the climate change history (Figure 4A, Table S1). Higher temperatures would slow the soil carbon accumulation on a global scale ($p < 0.05$), with a statistically significant average temporal temperature sensitivity (captures the dynamic response of soil carbon accumulation rates to climatic changes across time) of approximately −0.08 g·C·m^{-2}·yr^{-1}·°C^{-1} (Table S1). Typical soil profiles exhibited an inverse pattern between carbon CAR and temperature, with lower temperatures often associated with faster soil CARs (Figure 4B). This predominant impact of temperature on soil carbon sequestration is apparent both spatially and temporally.

The impact of temperature on carbon accumulation primarily operated through its effects on carbon inputs and outputs. To further explore the mechanisms, we analyzed the impact of temperature on the spatio-temporal dynamics of carbon inputs and outputs. As anticipated, warmer temperature was associated with larger carbon input and faster organic matter decomposition ($p < 0.05$, Figure S7). The influence of temperature on carbon outputs outweighed that on inputs, thus playing a dominant role in the present spatio-temporal pattern of carbon accumulation, with temperature primarily affecting decomposition processes. In other words, under conditions of continuous carbon input, the level of soil carbon accumulation was primarily determined by the rate of organic matter decomposition (output).[5] This mechanism was a well-recognized explanation for why the permafrost region represented the largest terrestrial carbon reservoir on Earth.[75–77]

Global carbon sequestration rate tends to decline over time

The global map of soil CARs was projected (Figure 5) based on the relationship between 18 predicted variables (Figure 3A) and soil CARs as modeled by Random-forest algorithms. The mean CAR in the boreal zone was 8.34 g·C·m^{-2}·yr^{-1}, more than 50% higher than the global mean CAR (5.25 g·C·m^{-2}·yr^{-1}) (Figure 5). Higher CARs were found in high-latitude wetland and tundra (Figure S8) compared to other vegetation types.

We reconstructed global CAR trajectories across the Holocene using the radiocarbon-based age framework of the compiled soil profiles (Figure S1A), which revealed biome-specific and non-linear patterns through time (Figure 6). Over the Holocene, mean CAR showed an overall decline, decreasing by approximately 3.39% (from 5.99 to 5.78 g·C·m^{-2}·yr^{-1}) at a global scale, 3.67% (from 9.97 to 9.60) for the boreal zone, and 4.91% (from 3.92 to 3.73) for the temperate zone, whereas CAR increased by 0.08%(from 3.291 to 3.294) for the tropical zone (Figure 6). We also forecasted future CAR trends up to the end of the 21^{st} century during the Anthropocene (Figure 6). By the mid-20th century, intensified anthropogenic activities began leaving a persistent signature on Earth, marking the proposed transition from the Holocene to the Anthropocene epoch. Rapid climate change is a defining feature of this new era.[78–80] We found that, by the end of this century, compared to current soil CAR (early Anthropocene, 1970–2000 AD), the average global soil CAR would decrease by 11% (with CAR% ranging from −69% to 46%) under the SSP126

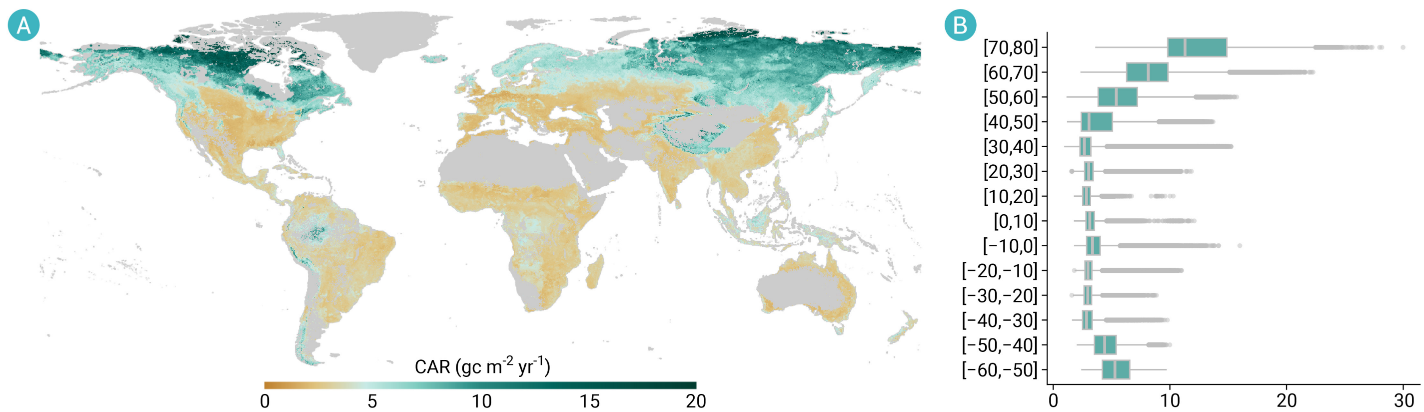

Figure 5. Global pattern of soil carbon accumulation rate (CAR) (A) Contemporary global distribution of CAR. (B) Latitudinal patterns of CAR at 10° intervals.

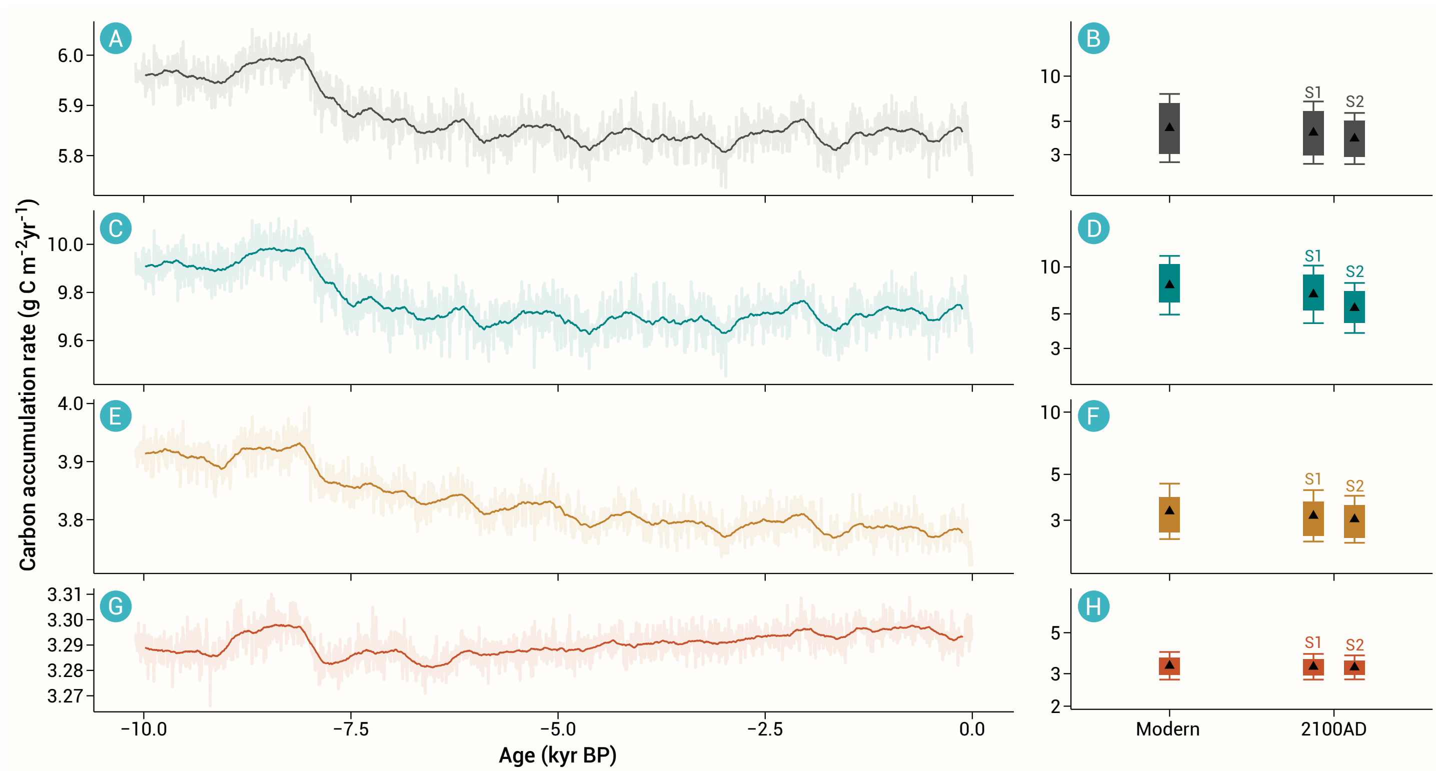

Figure 6. Temporal dynamics of carbon accumulation rate (CAR) since the start of the Holocene CAR dynamics over 10 kyr BP–0 BP, modern, and 2100 AD at the global scale (A–B), boreal zone (C–D), temperate zone (E–F), and tropical zone (G–H), respectively. Lines with lighter colors show time dynamics at 5-yr period, while darker lines show time dynamics with a 250-yr moving average through the data. Black triangles in boxplots denote the mean values, the boxes limit between the 25th and 75th percentiles, and whiskers indicate standard deviation range. Y axes of boxplots are at logarithmic scales. Figures S1-S2 indicate SSP126 and SSP585 scenarios, respectively.

scenario, and 18% (−78% ~ 50%) under the SSP585 scenario, with the most substantial reduction occurring above 50°N (Figures 7 & S9A).

DISCUSSION

Temperature exerts a predominant influence on the global spatio-temporal patterns of soil carbon accumulation, yet the observed regional distribution warrants further attention. In particular, high-latitude regions act as major historic carbon sinks and are highly vulnerable to future warming. This vulnerability could be driven by several interconnected factors. Firstly, organic matter decomposition in these areas has a higher temperature sensitivity.[81] And warming at rates higher than the global average substantially stimulates microbial activity that was limited by cold climate, leading to increased microbial respiration.[82] Second, many high-latitude forests are dominated by ectomycorrhizal (ECM) associations, warming may stimulate these fungi to produce oxidative enzymes that access previously protected soil organic matter pools, thereby supporting aboveground productivity but also accelerating soil carbon losses.[83,84] Third, soils in these regions have a higher proportion of easily decomposable POC compared to the more stable MAOC that predominates in tropical, the low-latitude areas (Figure S10).[83,85] This composition renders high-latitude soils particularly prone to climate-induced degradation of their carbon storage capabilities, resulting in a rapid decline in soil carbon accumulation rates. In contrast, low-latitude tropical region exhibits a positive CAR–MAT relationship. Such a pattern may arise because the warming-induced stimulation of carbon inputs outweighs its effect on carbon outputs. The underlying mechanisms likely include: (1) warming has increased net primary production, with prominent enhancements observed in tropical ecosystems,[86] thereby increasing litter and root inputs. Consistent with this mechanism, our analysis shows that CAR is positively related to belowground biomass in tropical regions with high root biomass (> ~20 Mg C ha^{-1}; Figure S4I), indicating that enhanced plant and root inputs may partly offset warming-induced decomposition;[87] (2) since microbial decomposition activity in the tropics is already near its thermal optimum, further warming may have a limited stimulatory effect on heterotrophic respiration;[88] and (3) the dominance of stable MAOC in tropical soils,[83] creates strong physico-

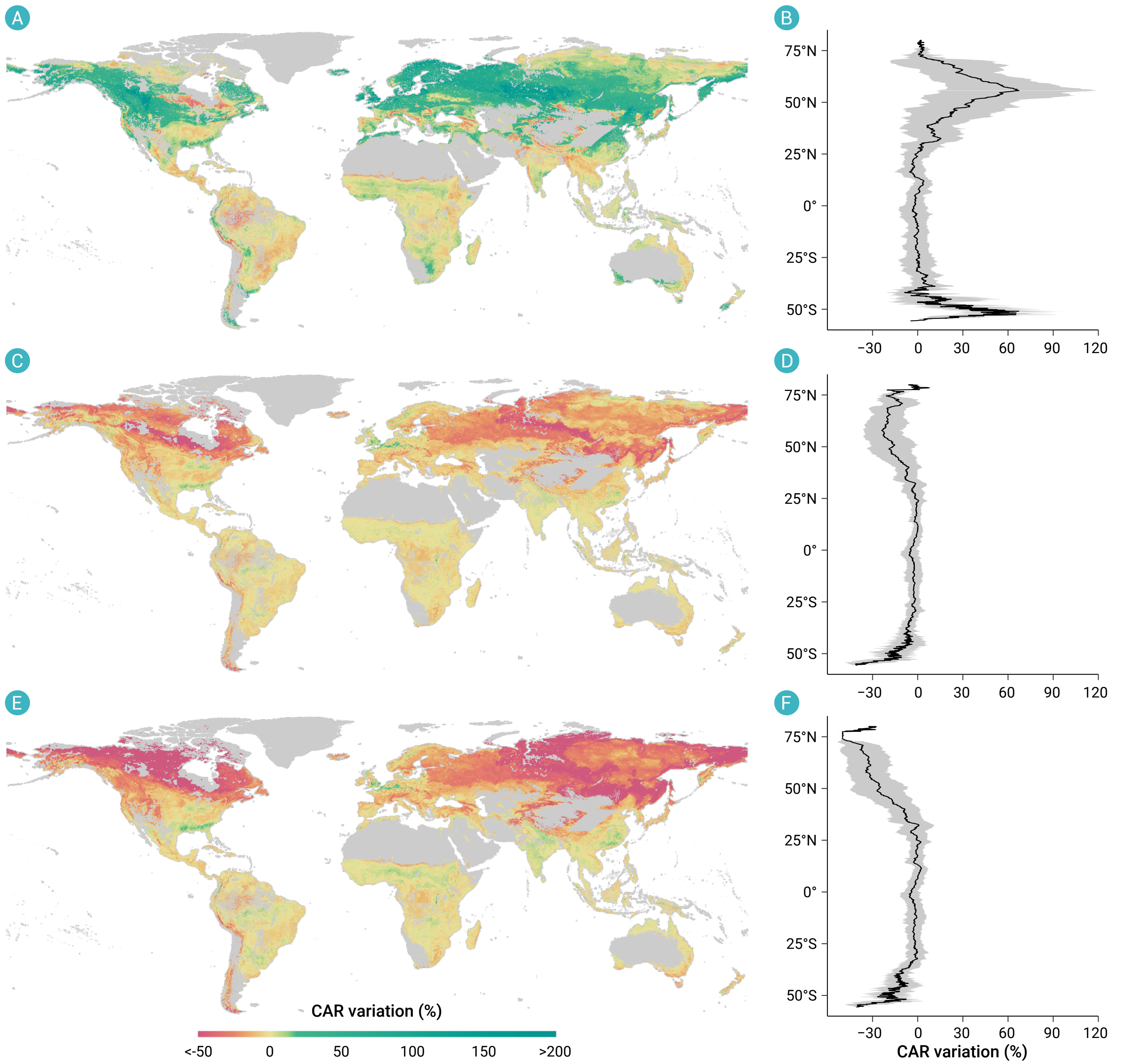

Figure 7. Global patterns of percentage changes in soil carbon accumulation rate (CAR%) across historical (5 kyr BP) and projected (2100AD) time periods in comparison to contemporary levels (A–B) Global patterns of CAR% change at 5 kyr BP versus modern. (C–D) Projected CAR% change in 2100 AD under SSP126. (E–F) Projected CAR% change in 2100 AD under SSP585. The shaded area of the latitudinal gradients of CAR% represents one standard deviation.

chemical barriers to microbial decay,[89] coupled with the prevalent periodic low-oxygen or fluctuating redox conditions,[90] suppress carbon oxidative processes. These mechanisms are widespread across tropical ecosystems and may collectively contribute to the consistent positive CAR–MAT relationship observed across spatial and temporal scales. However, despite the relatively high sensitivity of CAR to temperature, we observe only a slight increase in CAR during the Holocene, likely due to the limited magnitude of tropical Holocene warming relative to higher latitudes.[91]

While this study provides valuable insights into long-term global soil carbon dynamics, its methodological framework necessitates a cautious interpretation of the results. In this study, our predictions are based primarily on climate change, with other variables held constant, due to the current absence of globally consistent, time-varying datasets for these non-climatic predictors. This method may introduce significant uncertainties as key non-climatic variables can also play important roles in long-term soil carbon accumulation and change over millennial timescales. This is particularly relevant for variables associated with soil stabilization processes, which include physical occlusion within microaggregates and chemical sorption in organo-mineral complexes. These processes can limit the accessibility of microbial decomposers, thereby highlighting the significant influence of soil mineralogy on long-term carbon storage.[92] Growing evidence indicates that these mechanisms are climate-mediated. For instance, physical protection (e.g., aggregation) can be indirectly modulated by climate through its effects on soil texture and organic inputs.[93] Similarly, chemical protection, involving interactions between organic carbon and mineral ions (e.g., Fe, Ca), is influenced by climate-driven processes such as mineral weathering and transformation.[94] Thus, climate variables can indirectly reflect the temporal dynamics of these stabilization pathways. Moreover, the relative importance analysis shows that climatic variables are the predominant predictors of CAR, whereas proxies of soil stability (e.g., clay content, CEC) play secondary roles (Figure 3A). Therefore, we believe that climate-based predictions provide a feasible and justified framework for predicting CAR at global and millennial scales, though incorporating time-varying non-climatic datasets as they become available will further improve predictive accuracy.

Another concern arises from the analytical model and its applicability across diverse ecosystems. We employed the Bacon age–depth model—a framework predicated on monotonic carbon accumulation processes and widely applied in relatively closed ecosystems with negligible external carbon inputs[51]—to investigate spatio-temporal patterns of soil organic carbon accumulation. We acknowledge that extending this methodology to heterogeneous global ecosystems may introduce certain biases due to region-specific carbon accumulation mechanisms. Nevertheless, the robustness of our core conclusions is substantiated by the following methodological safeguards. Firstly, to address environmental heterogeneity in carbon accumulation processes, we validated our results using three independent methods: CLAM, nonlinear, and linear accumulation models (see details in Materials and Methods). The convergence of trends across all four analytical methods (including Bacon) reinforces the reliability of our findings (Figure S11). Secondly, in open ecosystems, where fresh organic matter from plant roots and dissolved organic carbon is continuously added to the soil, these inputs can influence the ^{14}C signal, rejuvenating carbon age in soils. To address this, we undertook several proactive measures to ensure the reliability of our results. We initially employed models, which effectively account for the contribution of recent plant-derived carbon[16] to calculate soil carbon age. We found that traditional dating methods, which do not account for surface carbon inputs, are highly correlated with the outputs of our one-pool model, although they tend to somewhat overestimate the soil carbon accumulation (Figure S12). We further excluded the uppermost 30 cm of soil profiles, the stratum most vulnerable to transient carbon fluxes and erosional effects. This exclusion preserved key spatial patterns in CAR and its relationship with temperature (Figures S13-S14), suggesting minimal long-term impacts of surface carbon inputs on deeper SOC stratigraphy. In other words, depth profiles can be translated into time when considering the vertical distribution of soil samples. Additionally, in wetland ecosystems where the probability of external fresh carbon input into the soil profile is low, we observed a significant negative correlation between mean annual temperature and CAR ($p < 0.01$; Figure S15), which aligns with findings in other open systems, further validating the reliability of our results. While sampled soils bear imprints of historical climate variability and disturbance regimes, the strong thermal modulation of SOC accumulation emerges as a statistically strong signal. This finding implies that depth-resolved SOC profiles retain centennial-to-millennial scale climatic information, with vertical stratigraphy serving as a temporal proxy. We emphasize that absolute CAR quantification remains challenging due to cumulative environmental perturbations. However, the consistency of thermal responses across analytical frameworks, ecosystem types, and depth profiles provides compelling evidence for the fundamental role of temperature in governing SOC accumulation dynamics. This mechanistic insight strengthens predictive models of soil carbon-climate feedbacks under future warming scenarios.

We also refer to other limitations in our analytical framework warrant targeted enhancements in future research. (1) Spatial representation gaps: Current datasets exhibit disproportionate coverage of temperate and boreal regions, while arid zones and tropical ecosystems remain underrepresented, potentially biasing global carbon accumulation patterns. (2) Landscape-scale processes: The aggregation of plot-scale measurements may obscure critical landscape controls, particularly in eroding systems where lateral carbon fluxes can exceed vertical accumulation. Emerging remote sensing platforms coupled with distributed hydrological modeling could bridge this scale gap. (3) Stabilization mechanism integration: While climate variables explain over 50% of CAR variability (Figure 3A), explicit incorporation of mineral protection processes (e.g., Fe–OC complexes)[95] and physical stabilization pathways (e.g., aggregate physical occlusion) into earth system models would enhance predictions across heterogeneous pedoclimatic regimes.

CONCLUSIONS

Using a global compilation of soil radiocarbon (^{14}C) measurements and soil carbon density, we quantified the temporal-spatial distribution of the soil carbon accumulation rates (CARs) over the Holocene and assessed these for recent changes in the Anthropocene. By reconstructing CAR at millennial timescales, we identified long-term, non-linear trajectories and biome-specific patterns that cannot be captured by simple linear extrapolation from short-term observations. Across these patterns, temperature emerges as a key driver of global CAR, with the cold zone having the highest soil CAR (8.4 $g\cdot C\cdot m^{-2}\cdot yr^{-1}$), compared to the warm tropical zone (3.3 $g\cdot C\cdot m^{-2}\cdot yr^{-1}$) and the temperate zone (3.1 $g\cdot C\cdot m^{-2}\cdot yr^{-1}$). Notably, the high-latitude regions, despite their crucial role in carbon sequestration indicated by faster soil CARs, are more vulnerable to future climate change, as suggested by the rapid decline in CARs as temperatures rise. These findings underscore the necessity for enhanced monitoring of soil carbon dynamics in high-latitude cold regions and the implementation of targeted conservation strategies to safeguard their substantial carbon stocks in the face of ongoing anthropogenic warming.

REFERENCES

1. Crowther T. W., Todd-Brown K. E. O., Rowe C. W., et al. (2016). Quantifying global soil carbon losses in response to warming. *Nature* **540**:104–108. DOI:10.1038/nature20150
2. Lal R. (2018). Digging deeper: A holistic perspective of factors affecting soil organic carbon sequestration in agroecosystems. *Glob. Chang. Biol.* **24**:3285–3301. DOI:10.1111/gcb.14054
3. Bradford M. A., Wieder W. R., Bonan G. B., et al. (2016). Managing uncertainty in soil carbon feedbacks to climate change. *Nat. Clim. Chang.* **6**:751–758. DOI:10.1038/nclimate3071
4. Bol R., Bolger T., Cully R., et al. (2003). Recalcitrant soil organic materials mineralize more efficiently at higher temperatures. *J. Plant Nutr. Soil Sci.* **166**:300–307. DOI:10.1002/jpln.200390047
5. Walker T. W. N., Kaiser C., Strasser F., et al. (2018). Microbial temperature sensitivity and biomass change explain soil carbon loss with warming. *Nat. Clim. Chang.* **8**:885–889. DOI:10.1038/s41558-018-0259-x
6. Gallego-Sala A., Charman D. J., Brewer S., et al. (2018). Latitudinal limits to the predicted increase of the peatland carbon sink with warming. *Nat. Clim. Chang.* **8**:907–913. DOI:10.1038/s41558-018-0271-1
7. Dungait J. A. J., Hopkins D. W., Gregory A. S., et al. (2012). Soil organic matter turnover is governed by accessibility not recalcitrance. *Glob. Chang. Biol.* **18**:1781–1796. DOI:10.1111/j.1365-2486.2012.02665.x
8. Piao S., Liu Q., Chen A., et al. (2019) Plant phenology and global climate change: Current progresses and challenges. *Glob. Chang. Biol.* **25**:1922–1940. DOI: 10.1111/gcb.14619
9. Nottingham A. T., Meir P., Velasquez E., et al. (2020). Soil carbon loss by experimental warming in a tropical forest. *Nature* **584**:234–237. DOI:10.1038/s41586-020-2566-4
10. Schiedung M., Don A., Beare M. H., et al. (2023). Soil carbon losses due to priming moderated by adaptation and legacy effects. *Nat. Geosci.* **16**:909–914. DOI:10.1038/s41561-023-01275-3
11. Todd-Brown K. E. O., Randerson J. T., Hopkins F., et al. (2014). Changes in soil organic carbon storage predicted by Earth system models during the 21st century. *Biogeosciences* **11**:2341–2356. DOI:10.5194/bg-11-2341-2014
12. Wang M., Guo X., Zhang S., et al. (2022). Global soil profiles indicate depth-dependent soil carbon losses under a warmer climate. *Nat. Commun.* **13**:5514. DOI:10.1038/s41467-022-33278-w
13. Soldatova E., Krasilnikov S. and Kuzyakov Y. (2024). Soil organic matter turnover: Global implications from $\delta^{13}C$ and $\delta^{15}N$ signatures. *Sci. Total Environ.* **912**:169423. DOI:10.1016/j.scitotenv.2023.169423
14. Sanderman J. (2018). Climate legacies drive global soil carbon stocks in terrestrial ecosystems. *Sci. Adv.* **4**:1–7. DOI:10.1126/sciadv.1701482
15. Fontaine S., Barot S., Barré P., et al. (2007). Stability of organic carbon in deep soil layers controlled by fresh carbon supply. *Nature* **450**:277–280. DOI:10.1038/nature06275
16. Shi Z., Allison S. D., He Y., et al. (2020). The age distribution of global soil carbon inferred from radiocarbon measurements. *Nat. Geosci.* **13**:555–559. DOI:10.1038/s41561-020-0596-z
17. Luo Z., Wang E., Sun O. J., et al. (2011). Modeling long-term soil carbon dynamics and sequestration potential in semi-arid agro-ecosystems. *Agric. For. Meteorol.* **151**:1529–1544. DOI:10.1016/j.agrformet.2011.06.011
18. Ren S., Wang T., Guenet B., et al., (2024). Projected soil carbon loss with warming in constrained Earth system models. *Nat. Commun.* **15**:1–10. DOI: 10.1038/s41467-023-44433-2
19. Ribeiro K., Pacheco F. S., Ferreira H. W., et al. (2021). Tropical peatlands and their contribution to the global carbon cycle and climate change. *Glob. Chang. Biol.*

27:489–505. DOI:10.1111/gcb.15408

20. Saito K., Machiya H., Iwahana G., et al. (2021). Numerical model to simulate long-term soil organic carbon and ground ice budget with permafrost and ice sheets (SOC-ICE-v1.0). 14:521–542. DOI: 10.5194/gmd-14-521-2021
21. Gao Y. and Couwenberg J. (2015). Carbon accumulation in a permafrost polygon peatland: Steady long-term rates in spite of shifts between dry and wet conditions. *Glob. Chang. Biol.* 21:803–815. DOI:10.1111/gcb.12742
22. Piilo S. R., Zhang H., Garneau M., et al. (2019). Recent peat and carbon accumulation following the Little Ice Age in northwestern Québec, Canada. *Environ. Res. Lett.* 14:075002. DOI:10.1088/1748-9326/ab11ec
23. Yu Z., Loisel J., Brosseau D. P., et al. (2010). Global peatland dynamics since the Last Glacial Maximum. *Geophys. Res. Lett.* 37:L13402. DOI:10.1029/2010GL043584
24. Todd-Brown K. E. O., Randerson J. T., Post W. M., et al. (2013). Causes of variation in soil carbon simulations from CMIP5 Earth system models and comparison with observations. *Biogeosciences* 10:1717–1736. DOI: 10.5194/bg-10-1717-2013
25. Wieder W. R., Bonan G. B. and Allison S. D. (2013) Global soil carbon projections are improved by modelling microbial processes. *Nat. Clim. Chang.* 3:909–912. DOI: 10. 1038/nclimate1951
26. He Y., Trumbore S. E., Torn M. S., et al. (2016). Radiocarbon constraints imply reduced carbon uptake by soils during the 21st century. *Science* 353:1419–1424. DOI:10.1126/science.aad4273
27. Li J., Yang S., Smith P., Li J., et al. (2025). Peak accumulation of soil organic carbon in the early Holocene. *Sci. Bull.* 70:2691–2700. DOI:10.1016/j.scib.2025.05.046
28. Lawrence C., Beem-Miller J., Hoyt A., et al. (2020). An open-source database for the synthesis of soil radiocarbon data: International soil radiocarbon database (ISRaD) version 1.0. *Earth Syst. Sci. Data.* 12:61–76. DOI: 10.5194/essd-12-61-2020
29. Kuneš P., Svobodová-Svitavská H., Kolář J., et al. (2015). The origin of grasslands in the temperate forest zone of east-central Europe: Long-term legacy of climate and human impact. *Quat. Sci. Rev.* 116:15–27. DOI:10.1016/j.quascirev.2015.03.014
30. Wang Y., Goring S. J. and McGuire J. L. (2019). Bayesian ages for pollen records since the last glaciation in North America. *Sci. Data* 6:1–8. DOI:10.1038/s41597-019-0182-7
31. Fick S. E. and Hijmans R. J. (2017). WorldClim 2: New 1-km spatial resolution climate surfaces for global land areas. *Int. J. Climatol.* 37:4302–4315. DOI:10.1002/joc.5086
32. Fordham D. A., Saltré F., Haythorne S., et al. (2017). PaleoView: A tool for generating continuous climate projections spanning the last 21 000 years at regional and global scales. *Ecography (Cop.).* 40:1348–1358. DOI:10.1111/ecog.03031
33. Tang W., Qin J., Yang K., et al. (2022). Mapping long-term and high-resolution global gridded photosynthetically active radiation using the ISCCP H-series cloud product and reanalysis data. *Earth Syst. Sci. Data* 14:2007–2019. DOI:10.5194/essd-14-2007-2022
34. Friedl M., Gray J. and Sulla-Menashe D. (2019). MCD12Q2 MODIS/Terra+Aqua land cover dynamics yearly L3 global 500m SIN grid v006 . *NASA Land Processes DACC.* DOI: 10.5067/MODIS/MCD12Q2.006
35. Zomer R. J., Xu J. and Trabucco A. (2022). Version 3 of the global aridity index and potential evapotranspiration database. *Sci. Data* 9:409. DOI:10.1038/s41597-022-01493-1
36. Zhao M. and Running S. W. (2010). Drought-induced reduction in global terrestrial net primary production from 2000 through 2009. *Science* 329:940–943. DOI:10.1126/ science.1192666
37. Spawn S. A., Sullivan C. C., Lark T.J., et al. (2020). Harmonized global maps of above and belowground biomass carbon density in the year 2010. *Sci. Data* 7:112. DOI:10. 1038/s41597-020-0444-4
38. Rabus B., Eineder M., Roth A., et al. (2003). The shuttle radar topography mission—A new class of digital elevation models acquired by spaceborne radar. *ISPRS J. Photogramm. Remote Sens.* 57:241–262. DOI:10.1016/S0924-2716(02)00124-7
39. Hengl T., Mendes de Jesus J., Heuvelink G. B. M., et al. (2017). SoilGrids250m: Global gridded soil information based on machine learning. *PLoS One* 12:e0169748. DOI:10. 1371/journal.pone.0169748
40. Poggio L., de Sousa L. M., Batjes N.H., et al. (2021). SoilGrids 2.0: Producing soil information for the globe with quantified spatial uncertainty. *SOIL* 7:217–240. DOI: 10. 5194/soil-7-217-2021
41. He L., Mazza Rodrigues J. L., Soudzilovskaia N. A., et al. (2020). Global biogeography of fungal and bacterial biomass carbon in topsoil. *Soil Biol. Biochem.* 151:108024. DOI:10.1016/j.soilbio.2020.108024
42. He L. and Xu X. (2021). Mapping soil microbial residence time at the global scale. *Glob. Chang. Biol.* 27:6484–6497. DOI:10.1111/gcb.15864
43. Torn M. S., Swanston C. W., Castanha C., et al. (2009). Storage and turnover of organic matter in soil. Senesi N., Xing B. and Huang P. M. (eds). Biophysico-Chemical processes involving natural nonliving organic matter in environmental systems (Wiley), pp:219–272. DOI: 10.1002/9780470494950.ch6
44. Reimer P. J., Baillie M. G. L., Bard E., et al. (2004). IntCal04 terrestrial radiocarbon age calibration, 0–26 cal kyr BP. *Radiocarbon* 46:1029–1058. DOI:10.1017/ S0033822200032999
45. Schuur E. A. G., Druffel E. and Trumbore S. E. (2016). Radiocarbon and climate change: Mechanisms, applications and laboratory techniques (Springer), pp:1–315. DOI:10.1007/978-3-319-25643-6
46. Chen L., Zhou G., Feng B., et al. (2024). Saline-alkali land reclamation boosts topsoil carbon storage by preferentially accumulating plant-derived carbon. *Sci. Bull.* 69:2948–2958. DOI:10.1016/j.scib.2024.03.063
47. Reimer P. J., Bard E., Bayliss A., et al. (2013). IntCal13 and marine13 radiocarbon age calibration curves 0–50,000 years cal BP. *Radiocarbon* 55:1869–1887. DOI:10.2458/ azu_js_rc.55.16947
48. von Fromm S. F., Hoyt A. M., Sierra C. A., et al. (2024). Controls and relationships of soil organic carbon abundance and persistence vary across pedo - climatic regions. *Glob. Chang. Biol.* 30:e17320. DOI:10.1111/gcb.17320
49. Xiao L., Wang G., Wang M., et al. (2022). Younger carbon dominates global soil carbon efflux. *Glob. Chang. Biol.* 28:5587–5599. DOI:10.1111/gcb.16311
50. Team R. C. (2013). R: A language and environment for statistical computing (R Foundation for Statistical Computing). https://cran.rstudio.com/manuals.html
51. Blaauw M. and Christen J. A. (2011). Flexible paleoclimate age-depth models using an autoregressive gamma process. *Bayesian Anal.* 6:457–474. DOI:10.1214/11-BA618
52. Hapsari K. A., Jennerjahn T. C., Lukas M.C., et al. (2020). Intertwined effects of climate and land use change on environmental dynamics and carbon accumulation in a mangrove-fringed coastal lagoon in Java, Indonesia. *Glob. Chang. Biol.* 26:1414–1431. DOI:10.1111/gcb.14926
53. Larsson A., Segerström U., Laudon H., et al. (2017). Holocene carbon and nitrogen accumulation rates in a boreal oligotrophic fen. *Holocene* 27:811–821. DOI:10.1177/ 0959683616675936
54. Batjes N. H., Ribeiro E., Van Oostrum A., et al. (2017). WoSIS: Providing standardised soil profile data for the world. *Earth Syst. Sci. Data* 9:1–14. DOI:10.5194/essd-9-1-2017
55. Hugelius G., Bockheim J. G., Camill P., et al. (2013). A new data set for estimating organic carbon storage to 3 m depth in soils of the northern circumpolar permafrost region. *Earth Syst. Sci. Data* 5:393–402. DOI:10.5194/essd-5-393-2013
56. Ding J., Wang T., Piao S., et al. (2019). The paleoclimatic footprint in the soil carbon stock of the Tibetan permafrost region. *Nat. Commun.* 10:1–9. DOI:10.1038/s41467-019-12214-5
57. Klaminder J., Yoo K. and Giesler R. (2009). Soil carbon accumulation in the dry tundra: Important role played by precipitation. *J. Geophys. Res. Biogeosciences* 114:G01007. DOI:10.1029/2009JG000947
58. Miller C. B., Rodriguez A. B., Mctigue N. D., et al. (2022). Carbon accumulation rates are highest at young and expanding salt marsh edges. *Commun. Earth Environ.* 3:1–9. DOI:10.1038/s43247-022-00501-x
59. Pries C. E. H., Schuur E. A. G. and Crummer K. G. (2012). Holocene carbon stocks and carbon accumulation rates altered in soils undergoing permafrost Thaw. *Ecosystems* 15:162–173. DOI:10.1007/s10021-011-9500-4
60. Torn M. S., Trumbore S. E., Chadwick O. A., et al. (1997). Mineral control of soil organic carbon storage and turnover. *Nature* 389:170–173. DOI:10.1038/38260
61. Blaauw M. (2010). Methods and code for "classical" age-modelling of radiocarbon sequences. *Quat. Geochronol.* 5:512–518. DOI:10.1016/j.quageo.2010.01.002
62. Blaauw M., Christen J. A., Bennett K. D., et al. (2018). Double the dates and go for Bayes — Impacts of model choice, dating density and quality on chronologies. *Quat. Sci. Rev.* 188:58–66. DOI:10.1016/j.quascirev.2018.03.032
63. Liaw A. and Wiener M. (2002). Classification and regression by randomForest. *R News* 2:18–22.
64. Breiman L. (2001). Random forests. *Mach. Learn.* 45:5–32. DOI:10.1023/A: 1010933404324
65. Díaz-Uriarte R. and Alvarez de Andrés S. (2006). Gene selection and classification of microarray data using random forest. *BMC Bioinformatics* 7:1–13. DOI:10.1186/1471-2105-7-3
66. Friedman J. H. (2001). Greedy function approximation: A gradient boosting machine. *Ann. Stat.* 29:1189–1232. DOI:10.1214/aos/1013203451
67. Bates D., Mächler M., Bolker, B., et al. (2015). Fitting linear mixed-effects models using lme4. *J. Stat. Softw.* 67:1–48. DOI:10.18637/jss.v067.i01
68. Adhikari K., Owens P. R., Libohova Z., et al. (2019). Assessing soil organic carbon stock of Wisconsin, USA and its fate under future land use and climate change. *Sci. Total Environ.* 667:833–845. DOI:10.1016/j.scitotenv.2019.02.420
69. Gray J. M., Bishop T. F. A. and Wilford J. R. (2016). Lithology and soil relationships for soil modelling and mapping. *Catena* 147:429–440. DOI:10.1016/j.catena.2016.07.045
70. Negassa M. K., Haile M., Feyisa G. L., et al. (2023). Soil organic carbon stock prediction: Fate under 2050 climate scenarios, the case of Eastern Ethiopia. *Sustain.* 15:1–23. DOI:10.3390/su15086495
71. Luo Z., Viscarra-Rossel R. A. and Qian T. (2021). Similar importance of edaphic and climatic factors for controlling soil organic carbon stocks of the world. *Biogeosciences* 18:2063–2073. DOI:10.5194/bg-18-2063-2021
72. Treat C. C., Kleinen T., Broothaerts N., et al. (2019). Widespread global peatland establishment and persistence over the last 130,000 y. *Proc. Natl. Acad. Sci. USA* 116:4822–4827. DOI:10.1073/pnas.1813305116
73. Mu M., Mu C., Liu H., et al. (2024). Topographic drivers of permafrost organic carbon accumulation on the northern Qinghai–Tibet Plateau. *Permafr. Periglac. Process.* 35:373–383. DOI:10.1002/ppp.2221
74. Li J., Zhu T., Singh B. K., et al. (2021). Key microorganisms mediate soil carbon-climate feedbacks in forest ecosystems. *Sci. Bull.* 66:2036–2044. DOI:10.1016/j.scib. 2021.03.008

75. Schuur E. A. G., Abbott B. W., Commane R., et al. (2022). Permafrost and climate change: Carbon cycle feedbacks from the warming Arctic. *Annu. Rev. Environ. Resour.* 47:343–371. DOI:10.1146/annurev-environ-012220-011847
76. Strauss J., Fuchs M., Hugelius G., et al. (2024). Organic matter storage and vulnerability in the permafrost domain. Elias S. A. (ed). Encyclopedia of Quaternary Science, 3rd Edition (Elsevier), pp:399–410. DOI: 10.1016/B978-0-323-99931-1.00164-1
77. Treat C. C., Virkkala A., Burke E., et al. (2024). Permafrost carbon: Progress on understanding stocks and fluxes across northern terrestrial ecosystems. *J. Geophys. Res. Biogeosciences* 129:e2023JG007638. DOI:10.1029/2023JG007638
78. Lewis S. L. and Maslin M. A. (2015). Defining the Anthropocene. *Nature* 519:171–180. DOI:10.1038/nature14258
79. Waters C. N., Steffen W., Waters C. N., et al. (2016). The Anthropocene is functionally and stratigraphically distinct from the Holocene. *Science* 351:aad2622. DOI:10.1126/science.aad2622
80. Zalasiewicz J., Waters C. N., Ellis E. C., et al. (2021). The Anthropocene: Comparing Its Meaning in Geology (Chronostratigraphy) with Conceptual Approaches Arising in Other Disciplines. *Earth's Futur.* 9:e2020EF001896. DOI:10.1029/2020ef001896
81. Koven C. D., Hugelius G., Lawrence D. M., et al. (2017). Higher climatological temperature sensitivity of soil carbon in cold than warm climates. *Nat. Clim. Chang.* 7:817–822. DOI:10.1038/nclimate3421
82. Wang C., Morrissey E. M., Mau R. L., et al. (2021). The temperature sensitivity of soil: Microbial biodiversity, growth, and carbon mineralization. *ISME J.* 15:2738–2747. DOI:10.1038/s41396-021-00959-1
83. Georgiou K., Jackson R. B., Vindušková O., et al. (2022). Global stocks and capacity of mineral-associated soil organic carbon. *Nat. Commun.* 13:1–12. DOI:10.1038/s41467-022-31540-9
84. Terrer C., Phillips R. P., Hungate B. A., et al. (2021). A trade-off between plant and soil carbon storage under elevated CO_2. *Nature* 591:599–603. DOI:10.1038/s41586-021-03306-8
85. Cotrufo M. F., Ranalli M. G., Haddix M. L., et al. (2019). Soil carbon storage informed by particulate and mineral-associated organic matter. *Nat. Geosci.* 12:989–994. DOI:10.1038/s41561-019-0484-6
86. Nemani R. R., Keeling C. D., Hashimoto H., et al. (2003). Climate-driven increases in global terrestrial net primary production from 1982 to 1999. *Science.* 300:1560–1563. DOI:10.1126/science.1082750
87. Zhou L., Zhou X., He Y., et al. (2022). Global systematic review with meta-analysis shows that warming effects on terrestrial plant biomass allocation are influenced by precipitation and mycorrhizal association. *Nat. Commun.* 13:4914. DOI:10.1038/s41467-022-32671-9
88. Qu L., Wang C., Manzoni S., et al. (2024). Stronger compensatory thermal adaptation of soil microbial respiration with higher substrate availability. *ISME J.* 18:wrae025. DOI:10.1093/ismejo/wrae025
89. Doetterl S., Stevens A., Six J., et al. (2015). Soil carbon storage controlled by interactions between geochemistry and climate. *Nat. Geosci.* 8:780–783. DOI:10.1038/ngeo2516
90. Bhattacharyya A., Campbell A. N., Tfaily M. M., et al. (2018). Redox fluctuations control the coupled cycling of iron and carbon in tropical forest soils. *Environ. Sci. Technol.* 52:14129–14139. DOI:10.1021/acs.est.8b03408
91. Liu Z., Zhu J., Rosenthal Y., Zhang X., et al. (2014). The Holocene temperature conundrum. *Proc. Natl. Acad. Sci. USA* 111:E3501–E3505. DOI:10.1073/pnas.1407229111
92. Hartley I. P., Hill T. C., Chadburn S. E., et al. (2021). Temperature effects on carbon storage are controlled by soil stabilisation capacities. *Nat. Commun.* 12:1–7. DOI:10.1038/s41467-021-27101-1
93. Lavallee J. M., Soong J. L. and Cotrufo M. F. (2020). Conceptualizing soil organic matter into particulate and mineral-associated forms to address global change in the 21st century. *Glob. Chang. Biol.* 26:261–273. DOI:10.1111/gcb.14859
94. Jia N., Li L., Guo H., et al. (2024). Important role of Fe oxides in global soil carbon stabilization and stocks. *Nat. Commun.* 15:10318. DOI:10.1038/s41467-024-54832-8
95. Ma T., Wang Y., Dai G., et al. (2025). Prolonged storage of bound organic carbon in wetland but not upland soils: A ^{13}C and ^{14}C Perspective. *Geophys. Res. Lett.* 52:e2024GL112491. DOI:10.1029/2024GL112491

FUNDING AND ACKNOWLEDGMENTS

This study was supported by the National Natural Science Foundation of China (42471159), the Second Tibetan Plateau Scientific Expedition and Research Program (2022QZKK0101), and the Chinese Academy of Sciences (CAS) Project for Young Scientists in Basic Research (YSBR-037). The funders had no role in study design, data collection and analysis, decision to publish, or preparation of the manuscript.

AUTHOR CONTRIBUTIONS

J.D. conceived the study. S.Y. and J.L. collected and processed the data. S.Y. analyzed the data and drafted the manuscript with considerable inputs from Y.K. and P.S. commented on the manuscript. All authors contributed to the interpretation of results of the manuscript.

DECLARATION OF INTERESTS

The authors declare no competing interests.

DATA AND CODE AVAILABILITY

Data are available from the corresponding author upon reasonable request.

SUPPLEMENTAL INFORMATION

It can be found online at https://doi.org/10.59717/j.xinn-geo.2026.100214.

LEAD CONTACT WEBSITE

Jinzhi Ding, https://itpcas.cas.cn/sourcedb_itpcas_cas/cn/expert/202010/t20201026_5722333.html